SLAC-PUB-11122
astro-ph/0503330

Draft version March 15, 2005
Preprint typeset using LaTeX style emulateapj v. 4/12/04

FORMING A PRIMORDIAL STAR IN A RELIC HII REGION

Brian O'Shea[1,2,3], Tom Abel[4], Dan Whalen[1,2] & Michael L. Norman[1]

Draft version March 15, 2005

ABSTRACT

There has been considerable theoretical debate over whether photoionization and supernova feedback from the first Population III stars facilitate or suppress the formation of the next generation of stars. We present results from an Eulerian adaptive mesh refinement simulation demonstrating the formation of a primordial star within a region ionized by an earlier nearby star. Despite the higher temperatures of the ionized gas and its flow out of the dark matter potential wells, this second star formed within 23 million years of its neighbor's death. The enhanced electron fraction within the HII region catalyzes rapid molecular hydrogen formation that leads to faster cooling in the subsequent star forming halos than in the first halos. This "second generation" primordial protostar has a much lower accretion rate because, unlike the first protostar, it forms in a rotationally supported disk of $\sim 10 - 100$ $M_\odot$. In contrast to unpreprocessed regions, such configurations may allow binaries or multiple systems of lower mass stars to form. These first high resolution calculations offer insight into the impact of feedback upon subsequent populations of stars and clearly demonstrate how primordial chemistry promotes the formation of subsequent generations of stars even in the presence of the entropy injected by the first stars into the IGM.

Subject headings: cosmology: theory — stars: formation — hydrodynamics

1. MOTIVATION

Calculations performed by Abel, Bryan and Norman (2002; hereafter ABN02) show that rapid accretion rates driven by molecular hydrogen cooling cause the formation of solitary massive protostars in the range of 30 to 300 $M_\odot$ in minihalos of $10^5 - 10^6$ $M_\odot$ at redshifts $\gtrsim 20$. Simulations indicate that the hard UV spectra of these 10^5 K zero-metallicity stars will envelop them in large HII regions several kiloparsecs in diameter (Whalen, Abel & Norman 2004; Kitayama et al. 2004). Over the main sequence lifetime of the central star (on the order of 2-6 Myr for the range of $30 - 300$ $M_\odot$) half of the baryons within the minihalo are driven beyond its virial radius by ionized flows that quickly steepen into shocks. These shocks exhibit expansion rates of up to ten times the escape velocity of the halo. After the death of the central star, cooling and recombination are out of equilibrium in the ionized gas, which results in significant electron fractions even after its temperature has dropped to 1000 - 2000 K after 20 - 50 Myr. One dimensional, nonrotating calculations (Heger et al. 2003) predict two possible fates for the primordial stars themselves: complete destruction by the pair instability (140 $M_\odot < M_* < 260$ $M_\odot$) which is very energetic and leaves no remnant, or direct collapse to black holes above and below this mass range, with the added possibility of SN-like precollapse mass ejections by pulsational pair instabilities from 100-140 $M_\odot$ stars (Heger & Woosley 2002).

An important question is whether later generations of stars can efficiently form in the relatively high temperatures and ionization fractions of the relic HII regions left by the first stars. One analytical study (Oh & Haiman 2003) found that the first stars injected sufficient entropy into the early IGM by photoheating and supernova explosions to prevent further local star formation in their vicinity. Lyman-Werner SUV background radiation is also thought to have contributed negative feedback by photodissociating primordial H_2 and quenching the molecular hydrogen cooling processes allowing the first stars to form (Haiman, Abel & Rees 2000; Machacek, Bryan & Abel 2001). In this *Letter* we present fully resolved simulations that show a second primordial star can form in the relic HII region of an earlier Pop III star. We determine its properties, considering the effect of Lyman-Werner radiation from the resultant black hole assuming accretion rates consistent with the density fields left by ionized outflows from the parent minihalo.

2. SIMULATION SETUP

We carried out simulations using Enzo, a publicly-available Eulerian adaptive mesh refinement (AMR) hydrodynamics + N-body code (Bryan & Norman 1997; O'Shea et al. 2004; also see http://cosmos.ucsd.edu/enzo). We initialized a box of size $300h^{-1}$ kpc at $z = 99$ for a cosmology with $(\Omega_M,\ \Omega_\Lambda,\ \Omega_B,\ h,\ \sigma_8,\ n) = (0.3, 0.7, 0.04, 0.7, 0.9, 1)$. We first ran a simulation with 128^3 dark matter particles in a 128^3 root grid with 6 total levels of adaptive mesh, refining on a dark matter overdensity of 4.0. This model was run with dark matter alone in order to identify the most massive halo that evolves in the simulation volume, which at $z \sim 18$ had a mass $\sim 5 \times 10^5 M_\odot$.

We then re-initialized the calculation in the original simulation volume at $z = 99$ with both baryons and dark matter using a 128^3 root grid and three static nested subgrids, each of which was twice as refined as its parent grid and was centered on the Lagrangian volume of the peak

[1] Center for Astrophysics and Space Sciences, University of California at San Diego, La Jolla, CA 92093, U.S.A. Email: bwoshea, mnorman, dwhalen@cosmos.ucsd.edu
[2] Department of Physics, University of Illinois in Urbana-Champaign
[3] Theoretical Astrophysics (T-6), Los Alamos National Laboratories
[4] Kavli Institute for Particle Astrophysics and Cosmology, Stanford University. Email: tabel@stanford.edu

Work supported in part by the Department of Energy contract DE-AC02-76SF00515

that later evolved into the identified halo. The effective root grid resolution was 1024^3 in this volume, which corresponds to a comoving spatial resolution of $\sim 300h^{-1}$ pc and a dark matter particle mass of $1.8h^{-1}M_\odot$ in the most highly refined region. Every dark matter particle that later enters into dark matter halos of interest was within this most highly refined grid at the start of the simulation.

We started the simulation with this set of initial conditions at $z = 99$ and followed the collapse of the first star, which occurred at a redshift of 17.76. As a refinement criteria we used a baryon overdensity of 4.0 and a dark matter overdensity of 8.0. In addition, to ensure appropriate simulation resolution we mandated that the Jeans length must be resolved by at least 16 cells at all times, which exceeds the Truelove criterion by a factor of 4 along each axis (Truelove et al. 1998). At the collapse redshift the three dimensional structure was resolved with 8727 grids on nine levels containing a total of 49,641,744 unique resolution elements.

To compute the extent of the HII region of the 120 $M_\odot$ Pop III star assumed to form in the collapse, we interpolated the density, energy, and velocity fields from the entire Enzo simulation volume at the formation redshift of this star onto a three dimensional grid of fixed resolution with 256^3 cells for import into a static radiative transfer code. The code utilizes the ionization front tracking technique of Abel (2000) to calculate the boundary of the HII region along rays cast outward from the central star by the adaptive ray tracing technique of Abel & Wandelt (2002). Within the HII region we set T = 10^4 K and set the ionization fraction equal to unity and H_2 and H^- fractions to zero.

We approximated the dynamics of the HII region by imposing the one dimensional velocity, ionization, density and temperature profiles for a 120 $M_\odot$ star at the end of its main sequence lifetime from Whalen et al. (2004) along every line of sight from the central star. We modified baryon densities and velocities out to ~ 120 pc (corresponding to the location of the shock wave in the 1D calculation) but changed only ionization fractions and temperatures beyond this radius out to the boundary of the HII region determined by the ray tracing code. We then mapped this HII region onto the full hierarchy of grids in the Enzo calculation, centering it on the location of the first protostar. This state corresponds to only 2.5 million years after the initial star formed (z $\simeq$ 17.4). We then continued the simulation until the collapse of the next protostar, which occurs at $z = 16.44$, 22.8 million years later. The final time that we analyzed contains 10,710 grid patches on 24 levels with 54,996,560 unique resolution elements. In this calculation we neglect the pulsational pair instability that may eject the hydrogen envelope for this star (Heger & Woosley 2002). The final result is insensitive to the mass of the star forming the HII region, however, as all stars in the ~ 100 $M_\odot$ range have similar lifetimes and UV fluxes.

As a check on our simulation setup we also ran a simulation where we simply instantaneously ionized the entire simulation volume by raising the baryon temperature to $\sim 10,000$ K and setting ionization fractions to one and H_2 fractions to zero. This simulation tests whether the addition of the one dimensional radial profiles from the Whalen et al. (2004) calculations changed the properties of the second protostar appreciably. We find that the collapse time and accretion rate of the protostar formed in this simulation are essentially identical to the results of our full setup, and only discuss results from the full setup in the rest of this *Letter*.

3. RESULTS

The second primordial protostar forms in a neighboring minihalo approximately 265 proper parsecs from the location of the halo in which the first star formed (and where the HII region originated). The halo in which this second protostar forms was completely ionized by the first star to a temperature of $\sim 10^4$ K. Due to its relatively high density, the center of this halo cools very rapidly and molecular hydrogen formation is catalyzed by the extremely high electron fraction. After only a few million years the core of the halo has a molecular hydrogen fraction of $\sim 5 \times 10^{-3}$, well above what one would expect for a halo which has not been ionized. This halo is significantly smaller than the first: $\sim 2 \times 10^5$ $M_\odot$ rather than $\sim 5 \times 10^5$ $M_\odot$.

3.1. *Comparison of the First and Second Stars*

Figure 1 compares the mass accretion times of the initial and second Population III stars formed in this simulation. In addition, this figure shows the mass accretion time of the halo in ABN02 and an estimate of the Kelvin-Helmholz timescale as a function of mass, using values of luminosity and effective temperature taken from Schaerer (2002). The upper and lower dotted lines correspond to an object with constant accretion rates of 10^{-3} and 10^{-2} $M_\odot$/year, respectively. Our calculation of accretion timescales for the initial protostar agrees well with that of ABN02. The fact that the two results are in good agreement even though the ABN02 calculations assumed a lower baryon fraction supports the analysis of Ripamonti and Abel (2004) showing that all mass scales in these calculations are set by molecular physics. Comparison of the accretion rates to the Kelvin-Helmholz timescale provides an estimate of ~ 200 $M_\odot$ for the upper bound of the mass of the star. The accretion timescales suggest a reasonable lower bound of ~ 80 $M_\odot$, since this much gas will accrete in 10^4 years, an insufficient time for fusion to begin. In contrast, the accretion rate of the second protostar is over an order of magnitude lower. This is because the second protostar has a much more pronounced thick disk structure than the first protostar. The disk is rotationally supported past a radius ~ 0.01 pc (corresponding to an enclosed mass of ~ 10 $M_\odot$), whereas the disk around the first star in the volume is not. Similar accretion timescale arguments as before suggest a mass of $\sim 5 - 20$ $M_\odot$ for the second star, although accretion physics will ultimately determine the true mass, particularly given the presence of this more pronounced disk.

3.2. *Black Hole Accretion*

Here we consider whether accretion onto a relic black hole could generate enough photodissociative radiation to inhibit H_2 formation in the second star's halo. We assume Bondi-Hoyle accretion (Bondi & Hoyle 1944) for the 120 $M_\odot$ black hole that forms after the collapse of the first star to estimate the Lyman-Werner flux from its accretion. This rate depends on the mass of the accretor as well as the local gas temperatures, densities,

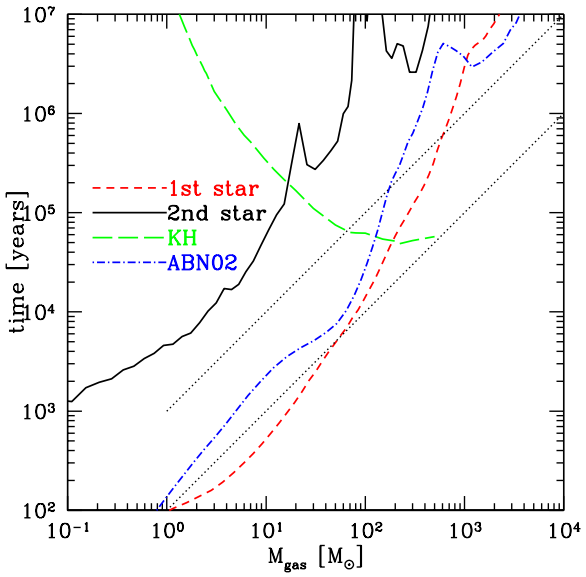

FIG. 1.— Mass accretion time $t_a = M(r)/\dot{M} \equiv M(r)/(4\pi r^2 \rho v_r)$ as a function of enclosed gas mass. This is at the final output corresponding to $z = 16.437$. The dashed line is the corresponding data dump of the initial star which had formed at $z = 17.67$. The red dashed line corresponds to the first star to form in this simulation. The blue dot-dashed line corresponds to the first star calculated in ABN02. The solid black line corresponds to the second star forming in this simulation, and the green long-dashed line corresponds to the Kelvin-Helmholz time of a representative star. The upper and lower black dotted lines correspond to objects with constant mass accretion rates of 10^{-2} and 10^{-3} $M_\odot$/yr, respectively.

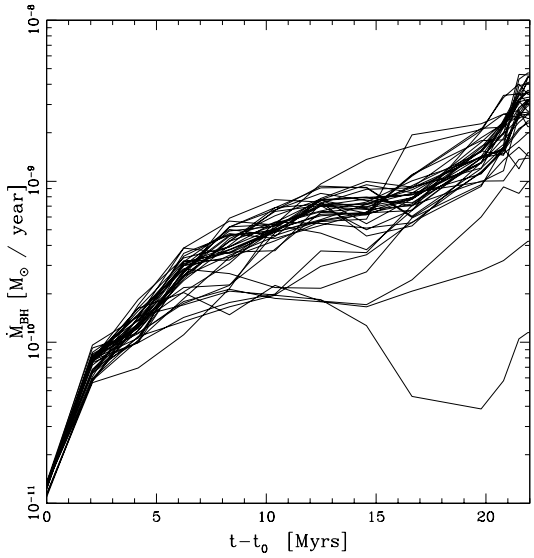

FIG. 2.— Bondi-Hoyle mass accretion rate around the black hole calculated from the local gas temperature, density and relative velocity. Integration of these curves lead to estimates of growth of the black hole (initially 120 $M_\odot$) of that range from 0.009 to 0.032 $M_\odot$ over 23 Myrs

and relative velocities it encounters. To sample the local environment the black hole would traverse over the duration of the simulation, we followed the 40 dark matter particles closest to the first protostar (within ~ 0.1 proper pc) from the end of its main sequence lifetime until the collapse of the second protostar. We tallied the cell quantities they crossed to compile the accretion rate history each particle would have if it were the black hole. The histories for the 40 black hole proxies appear in Figure 2. The mass accretion rates grow from 10^{-11} $M_\odot$/yr to $10^{-8.5}$ $M_\odot$/yr for most of the tracer particles.

To estimate the effect of Lyman-Werner radiation from the black hole on molecular hydrogen formation in nearby halos we assume a canonical 10% radiative efficiency for the accretion. The uppermost accretion curve yields $2.2 \times 10^{37}(M/100\ M_\odot)$ erg/s ($\sim 4500\ L_\odot$) for an upper limit to the total luminosity (which is much lower than the Eddington luminosity of this object, 1.5×10^{40} erg/s, or $\sim 4 \times 10^6\ L_\odot$). Taking this to be a blackbody spectrum, the flux in the Lyman-Werner band (11.1-13.6 eV) reaching the second protostar is $\sim 1.6 \times 10^{-25}(M/100\ M_\odot)$ erg s^{-1} cm^{-2} Hz^{-1}, resulting in photodissociation rates that are significantly lower than the formation rates of molecular hydrogen there. The expulsion of gas by ionized flows from the first halo prevents higher accretion rates and greater Lyman-Werner fluxes. A star in this mass range may shed its envelope just prior to collapse, resulting in a smaller black hole and making the results discussed here an upper limit.

4. DISCUSSION

This first high resolution three dimensional simulation of the evolution of gas within a primordial HII region demonstrates the crucial role of H_2 chemistry driven by photoionization in the formation of the next generation of stars. While this has been addressed in previous work (Ricotti, Gnedin & Shull 2002) our simulations are the first with high enough resolution to directly address the formation of individual stars. Further investigation will be necessary to determine if the lower accretion rates leading to the smaller mass of the second star are a coincidental feature of this calculation or a general trend of early star formation in halos preprocessed by HII regions. We note that our HII region enveloped roughly a dozen minihalos similar to the one that formed the second star. More calculations will be required to see if these too form stars. The evolution of the massive disk also merits examination to ascertain whether it breaks up into a multiple system or fully accretes to form a single star. Lower mass second generation stars or the possibility of binaries or multiple systems of primordial stars would have strong implications for the observability of such objects and their impact on subsequent structure formation. Less massive stars might have different nucleosynthetic signatures than those of the pair-instability supernovae that may occur in the first generation of primordial stars. The immense size of early HII regions could also make the scenario of primordial stars forming in a relic HII region much more common than extremely massive stars forming in pristine halos. These two facts taken together may account for the lack of detection of the characteristic odd-even abundance pattern from pair-instability supernovae expected in observations of ultra metal poor halo stars (Umeda & Nomoto 2005 and references therein). How HII regions from the first stars may regulate local star formation by suppressing the collapse of gas in local halos which have not reached relatively high densities also remains to be

explored.

BWO would like to thank Chris Fryer, Alex Heger and Falk Herwig for useful discussion. BWO, MLN and DW have been funded by NASA grant NAG5-12140 and NSF grant AST-0307690. BWO has been funded in part under the auspices of the U.S. Dept. of Energy, and supported by its contract W-7405-ENG-36 to Los Alamos National Laboratory. TA was supported by NSF CAREER award AST-0239709 from the National Science Foundation. The simulations were performed at SDSC and NCSA with computing time provided by NRAC allocation MCA98N020

REFERENCES

Abel, T. 2000, Revista Mexicana de Astronomia y Astrofisica Conference Series, 9, 300
Abel, T., Bryan, G. L., & Norman, M. L. 2002, Science, 295, 93
Abel, T. & Wandelt, B. D. 2002, MNRAS, 330, L53
Bondi, H. & Hoyle, F. 1944, MNRAS, 104, 273
Bryan, G. & Norman, M.L. 1997 In "Workshop on Structured Adaptive Mesh Refinement Grid Methods", Ed. N. Chrisochoides
Haiman, Z., Abel, T. & Rees, M. 2000, ApJ, 534, 11
Heger, A. & Woosley, S.E. 2002, ApJ, 567, 232
Heger, A., Fryer, C.L., Woosley, S.E., Langer, N. & Hartmann, D.H. 2003, ApJ, 591, 288
Kitayama, T., Yoshida, N., Susa, H., & Umemura, M. 2004, ApJ, 613, 631
Machacek, M.E., Bryan, G.L. & Abel, T. 2001, ApJ, 548, 509
Oh, S.P. & Haiman, Z. 2003 MNRAS, 346, 456
O'Shea, B.W., Bryan, G., Bordner, J., Norman, Michael L., Abel, T., Harknes, R. and Kritsuk, A. 2004. In "Adaptive Mesh Refinement - Theory and Applications", Eds. T. Plewa, T. Linde & V. G. Weirs, Springer Lecture Notes in Computational Science and Engineering
Ricotti, M., Gnedin, N.Y. & Shull, J.M. 2002b ApJ, 575, 49
Ripamonti, E. & Abel, T. 2004, MNRAS, 348, 1019
Schaerer, D. 2002, A&A, 382, 28
Truelove, J.K. et al. 1998, ApJ, 495, 821
Umeda, H. & Nomoto, K. 2005, ApJ, 619, 427
Whalen, D., Abel, T., & Norman, M. L. 2004, ApJ, 610, 14